The Astrophysical Journal, 976:27 (7pp), 2024 November 20 https://doi.org/10.3847/1538-4357/ad7f4f

Indirect Measurement of the ^{3}He(n,p)^{3}H Reaction Cross Section at Big Bang Energies

R. G. Pizzone[1,2], M. L. Sergi[1,2], A. A. Oliva[1,2], T. Zanatta-Martinez[1,2], L. Lamia[1,2], R. Spartá[1,2,3], G. L. Guardo[2], M. La Cognata[2], G. D'Agata[1,4], S. Palmerini[5,6], A. Tumino[2,3], M. Costa[2], D. Cittadino[2], A. Di Pietro[2], P. Figuera[2], I. Indelicato[2], A. Massara[2], S. Cherubini[1,2], G. G. Rapisarda[1,2], S. Romano[1,2], C. Spampinato[1,2], M. Couder[7], W. Tan[7], M. Wiescher[7], D. Lattuada[2,3], M. Gulino[2,3], V. Burjan[8], J. Mrazek[8], M. La Commara[9], M. Mazzocco[10], P. M. Prajapati[2,11], S. Aguilar[7], T. Anderson[7], D. Bardayan[7], D. Blankstein[7], L. Callahan[7], A. Clark[7], B. Frentz[7], A. Gula[7], M. Hall[7], S. L. Henderson[7], R. Kelmar[7], Q. Liu[7], J. Long[7], A. Majundar[7], S. McGiunness[7], A. Nelson[7], P. O'Malley[7], C. Seimour[7], M. Skulski[7], J. Wilkinson[7], S. M. Cha[12], K. Y. Chae[12], M. S. Kwag[12], and S. Typel[13,14]

[1] Dipartimento di Fisica e Astronomia "Ettore Majorana," Universitá di Catania, Catania, Italy; rgpizzone@lns.infn.it
[2] Laboratori Nazionali del Sud—INFN, Catania, Italy
[3] Facoltá di Ingegneria e Architettura, Universitá degli Studi di Enna Kore, Enna, Italy
[4] INFN, Sezione di Catania, Catania, Italy
[5] Dipartimentdo di Fisica e Geologia, Università degli Studi di Perugia, Perugia, Italy
[6] INFN Sezione di Perugia, Perugia, Italy
[7] Department of Physics & Astronomy, University of Notre Dame, South Bend, IN, USA
[8] Nuclear Physics Institute of the Czech Academy of Sciences, 250 68 Řež, Czech Republic
[9] Department of Pharmacy, University Federico II and INFN-Napoli, Napoli, Italy
[10] Universitá and Sezione di Padova—INFN, Padova, Italy
[11] Manipal Centre for Natural Sciences, Manipal Academy of Higher Education, Manipal—576104, India
[12] SKKU Sungkyunkwan University, Republic of Korea
[13] Technische Universität Darmstadt, Fachbereich Physik, Institut für Kernphysik, Darmstadt, Germany
[14] GSI Helmholtzzentrum für Schwerionenforschung GmbH, Theorie, Darmstadt, Germany

Received 2024 January 29; revised 2024 September 18; accepted 2024 September 23; published 2024 November 12

Abstract

Neutron-induced nuclear reactions play an important role in the Big Bang Nucleosynthesis. Their excitation functions are, from an experimental point of view, usually difficult to measure. Nevertheless, in the last decades, big efforts have led to a better understanding of their role in the primordial nucleosynthesis network. In this work, we apply the Trojan Horse Method to extract the cross section at astrophysical energies for the ^{3}He(n,p)^{3}H reaction after a detailed study of the ^{2}H(^{3}He,pt)H three-body process. Data extracted from the present measurement are compared with other published sets. The reaction rate is also calculated, and the impact on the Big Bang nucleosynthesis is examined in detail.

Unified Astronomy Thesaurus concepts: Big Bang nucleosynthesis (151)

1. Introduction

Hubble expansion, cosmic microwave background (CMB) radiation (G. Steigman 2007), and the Big Bang nucleosynthesis (BBN) model are considered the proof of the Big Bang models. The standard BBN is thought to have happened within 20 minutes after the Big Bang; thus, it constrains the Big Bang model at very early times, during the so-called radiation-dominated era.

According to the BBN model, starting from protons and neutrons, light nuclei (^{2}H,^{3,4}He,^{7}Li) are produced in predicted observable quantities. Great uncertainties affect both the ^{3}He abundance observation and the BBN-model estimates, as well as the attempt to estimate its primordial value. Thus, it is not used to validate the standard BBN model. The measured and BBN-model-calculated abundances of the remaining elements are consistent with the exception of ^{7}Li (G. Israelian 2012). This leads to the so-called "cosmological lithium problem."

The BBN model connects cosmology and nuclear physics (B. Fields & S. Sarkar 2006; A. Coc et al. 2011; R. H. Cyburt et al. 2016), the latter of which plays a crucial role in its description, and it is a well-established model that can reproduce all the primordial abundances by fixing only one parameter, usually the baryon-to-photon ratio η. That ratio is estimated by the precise analysis of the CMB ($\eta = 6.16 \pm 0.15 \times 10^{-10}$ from Planck E. Komatsu et al. 2011 is the value that is usually adopted), and its studies help constrain the BBN-model result when varying the rates of the reactions that played a major role (E. Kolb 2019). There are only 12 main reactions due to the relatively small amount of key nuclear species involved in BBN and its unique physical properties.

The reaction rates are calculated from the available low-energy reaction cross sections, and some of them are currently not known with sufficient precision, even though important achievements were reached in the last years (n_TOF Collaboration et al. 2016; V. Mossa et al. 2020; S. Hayakawa et al. 2021). Indeed, these reactions occurred at temperatures below $T_9 = 1$, and some of them involve neutrons and radioactive ions. In the last decades, these reactions have been widely studied, and in particular, great efforts have been devoted to their study by means of direct measurements at the relevant astrophysical energies, sometimes in underground laboratories (LUNA Collaboration et al. 1999; C. Rolfs 2001; C. Casella et al. 2002). They are also a fundamental input for a number of other still-unsolved astrophysical problems, e.g., the "lithium processing" either in the Sun or in other

Galactic stars (R. Weymann & E. Moore 1963; D. Ezer & G. W. Cameron 1962).

The ^{3}He(n,p)^{3}H reaction is a relevant neutron-induced process in BBN and has a strong impact on the primordial ^{3}He and ^{7}Li production. At the Big Bang temperatures, its reaction rate is mainly determined by the cross section in the energy range $0 \leqslant E_{\rm cm} \leqslant 0.4$ MeV. The first experimental measurement of its cross section was performed in the 1950s by J. H. Coon (1950) in the $0.1 \leqslant E_{\rm cm} \leqslant 30$ MeV using a neutron beam. Errors turned out to be around 30%. Other investigations at lower energies were conducted by J. H. Gibbons & R. L. Macklin (1959; inverse measurement); D. G. Costello et al. (1970), who measured in the range $0.3 \leqslant E_{\rm cm} \leqslant 1.1$ MeV; and R. Batchelor et al. (2004; direct measurement, $0.1 \leqslant E_{\rm cm} \leqslant 1$ MeV). In more recent years, theoretical predictions were also made available, with the most recent one carried out by M. Drosg & N. Otuka (2015), which covered a wider energy range.

Regarding the merely astrophysical purposes, reaction rates were then calculated by C. R. Brune et al. (1999), A. Adahchour & P. Descouvemont (2003), and M. S. Smith et al. (1993). They all show a similar trend at temperatures of astrophysical interest, while the reaction rate calculated by G. R. Caughlan & W. A. Fowler (1988) is considerably higher. However, in the energy range of interest for the BBN, the existing data are quite sparse. Moreover, most measurements occurred more than 50 yr ago, facing tough challenges in experiments, which still now are considerable. This gave rise to errors as high as 30%, depending on the energy where the measurement took place.

Alternative and complementary ways to obtain the cross section, σ, have been provided by indirect methods such as the Trojan Horse Method (THM; see C. Spitaleri et al. 2019 for a recent review), which is particularly suited to investigate, at astrophysical energies, binary reactions induced by neutrons or charged particles by using appropriate three-body reactions. The THM allows one to avoid both Coulomb and centrifugal barrier suppression and electron screening effects; thus, very low energies can be reached, and extrapolations are not needed. Moreover, it may be used with neutron-induced reactions and radioactive isotopes, as well as to determine cross sections of neutron-induced reactions on unstable isotopes. The THM in particular has shown its great power for measuring reaction rates for the BBN in the whole energy range of interest. This is reviewed in R. G. Pizzone et al. (2014) and has been extended to reactions induced by unstable nuclei of interest for BBN as in L. Lamia et al. (2017, 2019) and S. Hayakawa et al. (2021). The same methodology has been adopted for the ^{3}He(n,p)^{3}H reaction and will be reported in the present paper.

The first study of this reaction using the THM is described in R. G. Pizzone et al. (2020b). In the present paper, the full data sets taken in that experimental run were analyzed, and the overall results in improved statistics as well as a wider energy window where data are available. Moreover, reaction rates will be calculated, and the astrophysical implications discussed.

2. Trojan Horse Method: Generalities

The Trojan Horse Method (THM), first suggested by G. Baur et al. (1986) and C. Spitaleri (1991), then defined in the present formulation as reported in A. Tumino et al. (2021), aims at obtaining the cross section of the binary process $x + A \rightarrow b + B$ at astrophysical energies by studying a TH reaction, that is, a three-*particle* process $a + A \rightarrow b + B + s$, in the quasi-free (QF) kinematic regime. Under these conditions, the TH particle a, which has a dominant $s - x$ cluster structure, is propagating at energies above the Coulomb and centrifugal barriers and after penetration, undergoes breakup in the nuclear field of particle A. There, particle x interacts with target A, while cluster s, also called the *spectator*, flies away practically without changing its momentum. From the measured three-body cross section, the energy dependence of the binary subprocess $x + A \rightarrow b + B$ is determined. The QF reaction used to extract this cross section is schematically depicted for the binary reaction ^{3}He(n,p)^{3}H in Figure 1. For the details on the theoretical formalism, please refer to S. Typel & H. H. Wolter (2000), S. Typel & G. Baur (2003), C. Spitaleri et al. (2003), and references therein.

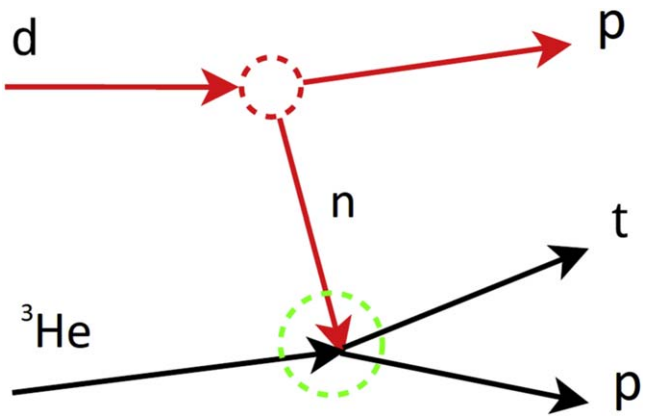

Figure 1. Diagrams describing the TH direct reaction ^{2}H(^{3}He,pt)H in the QF kinematics, proceeding through the ^{3}He(n,p)^{3}H subreaction.

This offers an intuitive explanation for the feasibility of exploring the entire Gamow window without necessitating extrapolation, using the THM approach. Moreover, as it is explained in detail in C. Spitaleri et al. (2019), a whole range of center-of-mass energies can be explored in correspondence with a single-beam of energy. However, a drawback of the current THM formulation is that the absolute value of the cross section must be established by adjusting the TH data to match available direct measurements, particularly at energies where electron screening effects are negligible. It is important to note that the $a + A \rightarrow b + B + s$ reaction can proceed through different reaction mechanisms besides QF so that an investigation of the process that is populating the $b + B + s$ final state is necessary before applying the THM approach. In particular, the QF reaction process gives a dominant contribution to the cross section in a restricted region of the three-body phase space, where the relative momentum p_{xs} of the fragments s and x is close to zero (QF kinematical condition) or $\hbar/p_{xs}$ is small compared to the bound state $s - x$ wavenumber. Owing to quantum mechanics, this entails the relative distance of x and s being very large, and we can assume that s acts as a spectator to the $x - A$ interaction, the strong interaction being of the short range.

The THM has proven its effectiveness in accurately determining cross sections for reactions involving charged particles at energies below the Coulomb barrier.

Many validity tests were also performed, like the pole invariance test, which was positively satisfied; for details, see R. G. Pizzone et al. (2013). The method has been used in the last three decades to explore nucleosynthesis reactions other than the primordial ones in different sites (e.g., L. Lamia et al. 2015; R. G. Pizzone et al. 2016; M. La Cognata et al. 2017; R. G. Pizzone et al. 2017; G. D'Agata et al. 2018).

In recent years, neutron-induced reactions (M. Gulino et al. 2010, 2013; G. L. Guardo et al. 2017, 2019) have been addressed as well, using deuterons as TH nuclei to transfer neutrons, while protons act as spectators. Following the simple plane-wave impulse approximation, the three-body reaction cross section of the reaction of interest can be factorized into three terms as:

$$\frac{d^3\sigma(E)}{d\Omega_\alpha d\Omega_{^3\mathrm{H}} dE_p} \propto \mathrm{KF} \cdot |\phi(p_s)|^2 \cdot \left(\frac{d\sigma}{d\Omega}\right)^{\mathrm{HOES}}, \quad (1)$$

where

(i) KF is a kinematical factor containing the final-state phase-space factor, which is a function of the masses, momenta, and angles of the outgoing particles;
(ii) $|\phi(p_s)|^2$ is the modulus-squared Fourier transform of the radial wave function $\chi(r_{p_n})$ describing the $p-n$ inter-cluster motion, given by the Hulthén function in terms of the spectator momentum p_s; and
(iii) $\left(\frac{d\sigma}{d\Omega}\right)^{\mathrm{HOES}}$ is the half-off-energy-shell (HOES) differential cross section of the reaction of interest at the center-of-mass energy E_{cm}.

The theory of the TH for resonant and nonresonant binary subreactions is presented in detail in R. E. Tribble et al. (2014). As it is sketched in Figure 1, this work will present the investigation of the ^{2}H(^{3}He,pp)^{3}H QF reaction, thus applying the THM in order to retrieve the cross section for the ^{3}He(n,p)^{3}H reaction at astrophysical energies.

3. Experiment Setup

The present work is based on the analysis of the coincidence between two of the three detectors of the experiment setup adopted and described in R. G. Pizzone et al. (2020b). A brief description is reported herein, but a more detailed one is present in the above reference. During the preparatory phase, detailed simulations were employed to identify the optimal angular and energy ranges, with the aim of enhancing the dominance of the QF reaction mechanism and minimizing interference from other processes within the target. Specifically, the QF angular pairs, which refer to angular combinations where the spectator momentum is close to zero, were computed.

The ^{3}He beam, delivered at a total kinetic energy of 9 MeV, was provided by the FN tandem accelerator at the Nuclear Science Laboratory of the University of Notre Dame. The total beam time lasted around 20 days including calibrations. The detectors were strategically positioned to encompass the specific kinematic region, as investigated in the preparatory simulations. In particular, three silicon position-sensitive detectors (PSDs 1–3), 1000 μm thick, were used; PSD1, which was aimed for triton detection, was coupled with a 35 μm thin, 10×50 mm^2 silicon detector for particle identification, while no particle identification was required for the other two detectors, thus optimizing the energy resolution of the apparatus. The spatial resolution of the PSD is below 1 mm, giving rise, for the considered detector distances, to an angular resolution around 0.°15–0.°2. The detector's energy resolution is around 0.8%. Two symmetrical monitor detectors were placed on both sides of the beam at 60° to check its symmetry. Another point-like silicon detector (point-like (PL1)) was placed at 45° for online monitoring of the deuterated polyethylene target thickness and its deuterium content during the experiment. A metal grid, with equally spaced slits, was placed in front of each PSD in order to perform an accurate angular calibration. The angular positions of the detectors are summarized in Table 1. Various thicknesses of isotopically enriched (up to 98%) deuterated polyethylene targets have been employed. Such targets were manufactured at the INFN-LNS target laboratory.

Table 1
Angular Position, Distance, and Covered Angular Range from the Central Position of the PSD1, PSD2, PSD3, and ΔE_1 Detectors as Described in the Text

ID	Central Angle (deg)	Distance (cm)	$\Delta\theta$ (deg)
PSD1	10.0	35	±4
PSD2	−15.0	20	±7
PSD3	−25.0	35	±4
ΔE$_1$	10.0	33	±4.3

After the initial calibration runs for energy and angular calibration (where an overall angular resolution of 0.°1 was achieved), coincidence data between PSD1 and PSD2 or between PSD1 and PSD3 were taken. The present work will deal with the analysis of one part of the overall data acquired in the experimental run. In particular, the PSD1–PSD3 coincidence will be examined here while data arising from the PSD1–PSD2 coincidence were discussed in R. G. Pizzone et al. (2020b). The present kinematic conditions explore higher energies in the E_{cm} range with respect to the PSD1–PSD2 coincidence, thus giving the opportunity of studying a complementary and more extended range with respect to R. G. Pizzone et al. (2020b).

4. Data Analysis

The first step of the data analysis is the identification of the three-body process of interest among those occurring in the target, leading to the detection in coincidence of two particles in two out of the three detectors. For this purpose, a particle identification is performed for PSD1 via the $\Delta E/E$ technique as reported in R. G. Pizzone et al. (2020b) by making a graphical cut on the tritium particles in the ΔE–E spectrum.

In the scatterplot in Figure 2, the kinematic locus of the t particle detected in PSD1 and coincidences in PSD3 (red points) is compared with a Monte Carlo simulation for the same conditions. A clear agreement is evident in the whole explored energy range and for the different angular pairs examined, giving strong proof that the particles detected in PSD3 are protons and the examined process is the ^{2}H(^{3}He,pt)H reaction of interest.

Once the angle and energy of the two detected particles are calibrated, the energy and the angle of the third, undetected, particle is reconstructed from energy and momentum conservation. This allows us to extract the Q-value of the three-body reaction as shown in Figure 3. A Gaussian fit gives a value of -1.50 ± 0.1 MeV, which should be compared with an expected value of $Q = -1.46$ MeV, obtained with Qtool (R. MacFarlane & P. Moller 1997). The agreement between expected and measured values in Figures 2 and 3 validates the energy calibration. Henceforth, only events with $-1.7 \leqslant Q \leqslant -1.4$ MeV will be considered for further analysis, thus leading to a clear identification of the ^{2}H(^{3}He,pt)H process.

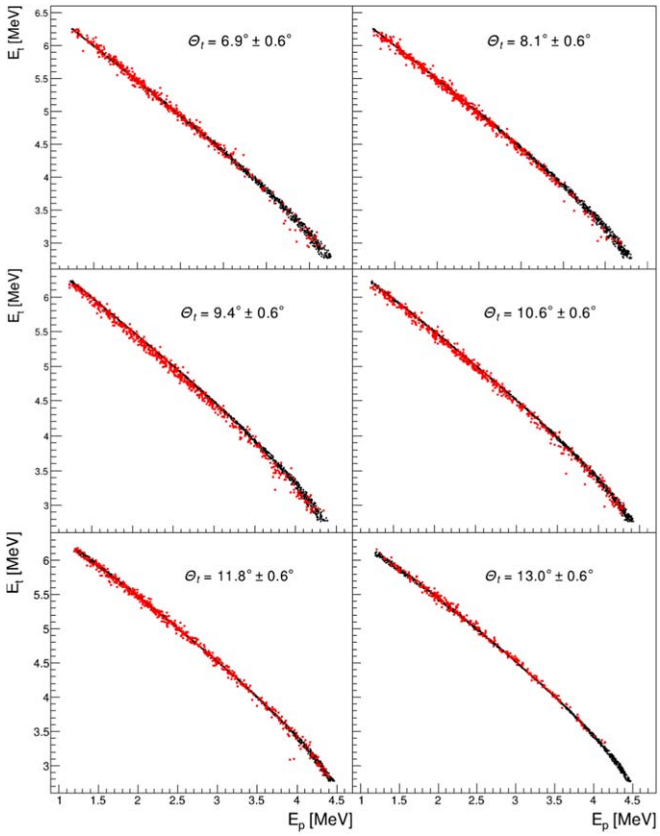

Figure 2. Kinematic locus for tritons detected in PSD1 and protons from PSD3 for $6.^{\circ}3 \leqslant \theta_t \leqslant 13.^{\circ}6$ and $24.^{\circ}4 \leqslant \theta_p \leqslant 25.^{\circ}6$, respectively. The experimental data for tritium events (red circles) are compared with a kinematical Monte Carlo simulation (black dots) for the ^{2}H(^{3}He,pt)H reaction.

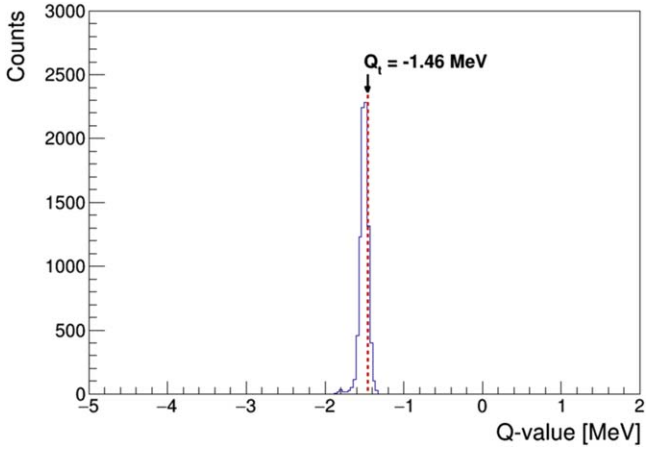

Figure 3. Q-value spectrum for PSD1–PSD3 coincidences after tritons are selected in PSD1. The calculated value of −1.46 MeV is in fair agreement and is indicated by the red line corresponding to the black arrow.

4.1 Identification of the WF Breakup

The next step in the data analysis is the identification of the QF mechanism and, consequently, its separation from other processes, e.g., sequential decay, which may occur in the beam target interaction. After studying the relative energy correlation plots as in L. Lamia et al. (2009), we can exclude the presence of any sequential mechanism leading to ^{4}He particles in the final state. This is evident in Figure 4, where no horizontal loci

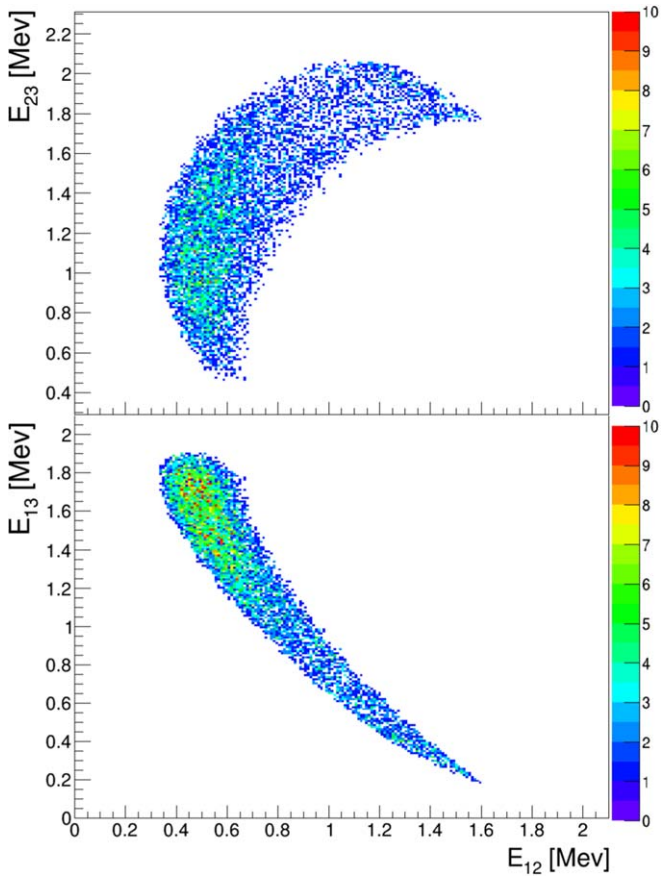

Figure 4. Relative energy spectra. No levels connected to the coincidence ^{3}H + p (particles 1–3) are evident as horizontal lines.

for the relative energy between particles 1 and 3, (indicated with E_{13}), corresponding to states in ^{4}He, are present, giving proof that no sequential decay is present.

Hence, to verify whether the QF process is taking place or not, the extraction of the momentum distribution of the spectator proton inside the TH nucleus (deuteron) has to be extracted and carefully analyzed.

The momentum distribution is extracted following the prescriptions of R. G. Pizzone et al. (2020a); inverting Equation (1) in terms of the momentum distribution leads to

$$|\phi(p_s)|^2 \propto \frac{d^3\sigma(E)}{d\Omega_\alpha d\Omega_{^7\mathrm{Li}} dE_\alpha} \Big/ \mathrm{KF} \cdot \left(\frac{d\sigma}{d\Omega}\right)^{\mathrm{HOES}}. \quad (2)$$

Assuming a narrow energy interval ($\Delta E_{\mathrm{cm}} = 200$ keV in the present case), the binary HOES cross section is almost constant. Therefore, by dividing the triple differential cross section by the kinematic factor, KF, the momentum distribution $|\phi(p_s)|^2$ in arbitrary units can be obtained. This latter quantity is plotted in Figure 5. A Gaussian fit is superimposed in red (FWHM $= 42 \pm 5$ MeV c^{-1}), while the black line represents the theoretical Hulthén function as discussed in L. Lamia et al. (2012). It is evident that the present momentum distribution is distorted and narrower, an effect already pointed out for deuteron and other nuclides in R. G. Pizzone et al. (2020a). In fact, in this case, a transferred momentum $q_t = 80$ MeV c^{-1} is calculated, and the corresponding momentum-distribution width fits pretty well with what is reported in the literature for the deuteron acting as the Trojan horse nucleus (R. G. Pizzone et al. 2020a). This is coherent with the results obtained for

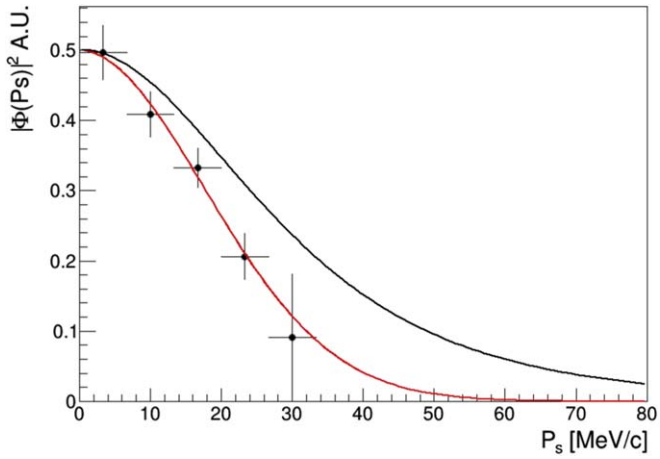

Figure 5. Momentum distribution in arbitrary units for the proton inside the TH deuteron. A Gaussian fit is depicted (red line), together with the theoretical momentum distribution given by the Hulthén function (black solid line).

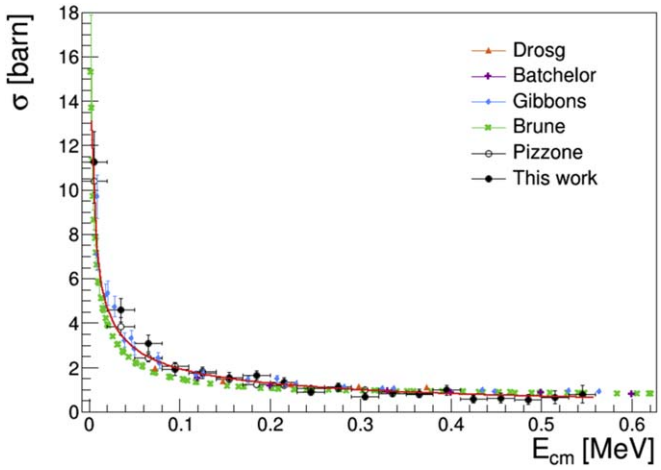

Figure 6. Binary cross section (black circles) after including the penetration factor and normalized to direct data from M. Drosg & N. Otuka (2015), R. Batchelor et al. (2004), J. H. Gibbons & R. L. Macklin (1959), R. G. Pizzone et al. (2020b), and C. R. Brune et al. (1999) for the ^{3}He(n,p)^{3}H subreaction extracted via the TH reaction ^{2}H(^{3}He,pt)H in QF kinematics, as discussed in the text. Errors from statistics and normalization are shown. The red curve represents the $1/v$ trend and is reported for comparison.

deuteron breakup reported in R. G. Pizzone et al. (2020b). In the present case, both statistical and systematic errors are considered.

For further analysis, only events with $p_s \leqslant 25$ MeV c^{-1} were taken into account, which were the bulk of the QF contribution in the ^{2}H(^{3}He,pt)H process.

5. Results and Astrophysical Considerations

After the selection of events related to the QF breakup, standard THM prescriptions are followed. Using the postcollision approach for the definition of $E_{\rm cm} = E_{12}$–Q_{2b} (where Q_{2b} is the two-body reaction Q-value), the triple differential cross section is divided by the $KF \cdot |\phi(p_s)|^2$ factor, according to Equation (1). As shown in R. G. Pizzone et al. (2020a) the distorted momentum distribution, which has been measured experimentally in this present case, is used. The result gives the HOES binary cross section for the ^{3}He(n,p)^{3}H reaction in

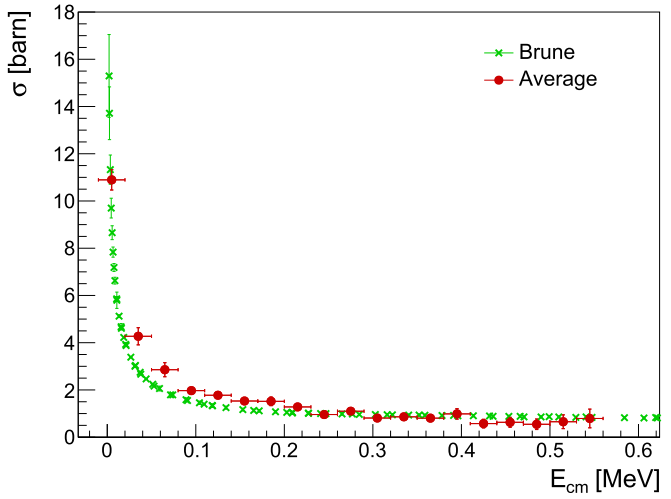

Figure 7. Average binary cross section (red circles, average of present data and R. G. Pizzone et al. 2020b) for the ^{3}He(n,p)^{3}H subreaction extracted via the TH reaction ^{2}H(^{3}He,pt)H, as discussed in the text. Errors from statistics and normalization are shown. Direct data from C. R. Brune et al. (1999) are reported for comparison.

arbitrary units. The THM data must be multiplied for the penetration factor in order to be compared and normalized to on-shell, direct data. In this case, the same procedure adopted in M. Gulino et al. (2010, 2013) was applied.

The results after applying this correction are shown in Figure 6 together with direct data. The cross section was normalized to the direct data from M. Drosg & N. Otuka (2015), R. Batchelor et al. (2004), and J. H. Gibbons & R. L. Macklin (1959) in the energy range $0.3 \leqslant E_{\rm cm} \leqslant 0.6$ MeV, as it is reported in Figure 6. A good agreement within the experimental uncertainties shows up in the whole examined energy range. Statistical errors as well as errors arising from normalization to the direct data were fully taken into account, yielding a maximum 10% relative error for the THM cross section. As far as the error on the quantities contributing to $E_{\rm cm}$, we apply the error-propagation law assuming an uncertainty on E_p and E_t of 0.8% and an error on the position $\Delta\theta_p \approx \Delta\theta_t \approx 0.^{\circ}15$.

The present data confirm the $1/v$ behavior at low energies and allow the extension of the explored energy range reported in R. G. Pizzone et al. (2020b) to higher energies. An overall average of the two data sets was then made and the result is given in Figure 7, and it is compared to the available direct data. Once more, the method has proved to be important for measuring neutron-induced reactions of astrophysical interest at thermal energies. The present data set confirms, within the experimental errors, a very satisfying agreement of the measured data with direct and inverse reaction data from the literature (J. H. Gibbons & R. L. Macklin 1959; C. R. Brune et al. 1999; R. Batchelor et al. 2004; M. Drosg & N. Otuka 2015) in the energy region $0.03 \leqslant E_{\rm cm} \leqslant 0.6$ MeV. A slight discrepancy with the experimental trend of the data reported by C. R. Brune et al. (1999) is present in the energy range between 60 and 200 keV. We also underline that the present data are the only ones, besides those from J. H. Gibbons & R. L. Macklin (1959) and C. R. Brune et al. (1999), available below 0.1 MeV.

As a last point of the data analysis, the reaction rate (expressed in cm^{3} mol^{-1} s^{-1}) for the ^{3}He(n,p)^{3}H reaction was

Table 2
Reaction Rate for the ^{3}He(n,p)^{3}H Reaction in cm^{-3} s^{-1}mol^{-1} (Average, Upper Limit, and Lower Limit) according to the Present Measurement

T	Rate$_{lower}$	Rate$_{avg}$	Rate$_{upper}$
0.1	7.54E+08	7.94E+08	8.34E+08
0.2	7.48E+08	7.99E+08	8.49E+08
0.3	7.17E+08	7.70E+08	8.23E+08
0.4	6.90E+08	7.42E+08	7.93E+08
0.5	6.69E+08	7.18E+08	7.68E+08
0.6	6.51E+08	6.99E+08	7.47E+08
0.7	6.35E+08	6.82E+08	7.28E+08
0.8	6.21E+08	6.67E+08	7.13E+08
0.9	6.08E+08	6.53E+08	6.99E+08
1	5.95E+08	6.41E+08	6.87E+08
1.1	5.83E+08	6.29E+08	6.76E+08
1.2	5.71E+08	6.18E+08	6.66E+08
1.3	5.59E+08	6.07E+08	6.56E+08
1.4	5.47E+08	5.97E+08	6.47E+08
1.5	5.35E+08	5.86E+08	6.38E+08
1.6	5.23E+08	5.76E+08	6.29E+08
1.7	5.12E+08	5.66E+08	6.20E+08
1.8	5.01E+08	5.56E+08	6.11E+08
1.9	4.89E+08	5.46E+08	6.02E+08
2	4.78E+08	5.36E+08	5.93E+08
2.1	4.68E+08	5.26E+08	5.84E+08
2.2	4.57E+08	5.16E+08	5.75E+08
2.3	4.47E+08	5.07E+08	5.66E+08
2.4	4.37E+08	4.97E+08	5.57E+08
2.5	4.27E+08	4.88E+08	5.48E+08
2.6	4.17E+08	4.78E+08	5.40E+08
2.7	4.08E+08	4.69E+08	5.31E+08
2.8	3.99E+08	4.60E+08	5.22E+08
2.9	3.90E+08	4.52E+08	5.13E+08
3	3.81E+08	4.43E+08	5.05E+08
3.1	3.73E+08	4.35E+08	4.96E+08
3.2	3.65E+08	4.26E+08	4.88E+08
3.3	3.57E+08	4.18E+08	4.80E+08
3.4	3.49E+08	4.11E+08	4.72E+08
3.5	3.42E+08	4.03E+08	4.64E+08
3.6	3.35E+08	3.95E+08	4.56E+08
3.7	3.28E+08	3.88E+08	4.48E+08
3.8	3.21E+08	3.81E+08	4.41E+08
3.9	3.14E+08	3.74E+08	4.33E+08
4	3.08E+08	3.67E+08	4.26E+08
4.1	3.02E+08	3.60E+08	4.19E+08
4.2	2.96E+08	3.54E+08	4.12E+08
4.3	2.90E+08	3.48E+08	4.05E+08
4.4	2.84E+08	3.41E+08	3.98E+08
4.5	2.79E+08	3.35E+08	3.92E+08
4.6	2.74E+08	3.30E+08	3.85E+08
4.7	2.68E+08	3.24E+08	3.79E+08
4.8	2.63E+08	3.18E+08	3.73E+08
4.9	2.58E+08	3.13E+08	3.67E+08
5	2.54E+08	3.08E+08	3.61E+08

Note. The temperature (first column) is given in units of T_9.

calculated according to the standard expression

$$N_A\langle\sigma v\rangle = \frac{\alpha}{T_9^{3/2}}\sqrt{\mu}\cdot\int_0^{\infty} E\sigma(E)\exp\left(\frac{-11.605E}{T_9}\right)dE, \quad (3)$$

with $\alpha = 3.7318\times10^{10}$ and μ the reduced mass in a.m.u. (atomic mass unit) and where the center-of-mass energy E is in units of MeV, the temperature is T_9, and the cross section is σ in barns. The result is reported in terms of its average, with the lower and upper values in Table 2, and it is plotted in Figure 8

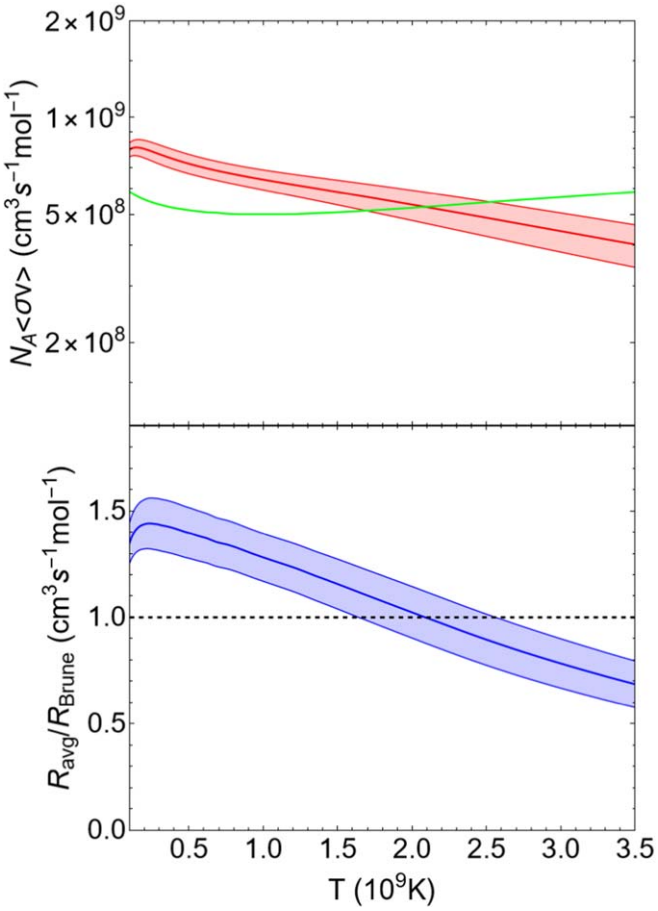

Figure 8. Reaction rate for the ^{3}He(n,p)^{3}H reaction (red curve, upper panel). The green line (upper panel) represents the reaction rate calculated by C. R. Brune et al. (1999). In the lower panel, the ratio of the present rate with respect to the one calculated in C. R. Brune et al. (1999) is reported. The shaded area takes into account the uncertainties.

Table 3
Primordial Abundances Calculated for Different Isotopes with the Reaction Rates Present in C. Pitrou et al. (2018)

Isotope	C. Pitrou et al. (2018)	This Work
^{4}He	0.247	0.247
^{3}He/H $\times 10^5$	1.066	0.996
(^{3}He + ^{3}H)/H $\times 10^5$	1.074	1.004
^{7}Li/H $\times 10^{11}$	2.889	2.876
(^{7}Li+^{7}Be)/H $\times 10^{10}$	5.670	5.134

Note. In the third column, the reaction rate for the ^{3}He(n,p)^{3}H reaction is taken for the present work. For reference, the observed abundance of primordial Li is $1{,}58^{\pm0,3}$ (M. Pettini et al. 2008).

as a function of the temperature. In the upper panel, the reaction rate is reported, while the lower panel shows the ratio of the present calculation with the rate calculated by C. R. Brune et al. (1999). An overall agreement is present even though increases in reaction rate up to a factor of 30% are present in the energy window of astrophysical interest.

The present value of the reaction rate for the ^{3}He(n,p)^{3}H reaction was then used in a primordial nucleosynthesis code PRIMAT (C. Pitrou et al. 2018) and substituted with the one present in the network of the code. The results of the calculation are reported in Table 3 in terms of the calculated

primordial abundance of the different isotopes. Although the ^{7}Li abundance with present changes in reaction rate goes to smaller values, the discrepancy with the observed values ($^7\mathrm{Li/H} \times 10^{-10} = 1.58^{\pm 0,3}$; M. Pettini et al. 2008) is still far from being explained. Once more, it seems that the roots of these discrepancies should be found in other processes, i.e., stellar lithium processing especially for Population II stars (A. J. Korn et al. 2006).

Acknowledgments

We thank the staff of the LNS target laboratory for target preparation, as well as the Nuclear Science Laboratory (supported by grant the National Science Foundation under grant No. NSF PHY-1713857) staff at the University of Notre Dame for their invaluable efforts. J.M, G.D., and V.B. were supported by MEYS Czech Republic under the project EF16-013/0001679. The authors acknowledge "Piano Incentivi per la ricerca PIACERI 2024-26 " Linea di Intervento 1 “Progetti di ricerca collaborativa" by University of Catania. This work was also supported in part by the National Research Foundation of Korea (NRF) grant funded by the Korea government (MSIT) (Nos. 2020R1A2C1005981 and 2016R1A5A1013277).

ORCID iDs

R. G. Pizzone https://orcid.org/0000-0003-2436-6640

References

Adahchour, A., & Descouvemont, P. 2003, JPhG, 29, 395
Batchelor, R., Aves, R., & Skyrme, T. H. R. 2004, RScI, 26, 1037
Baur, G., Bertulani, C. A., & Rebel, H. 1986, NuPhA, 458, 188
Brune, C. R., Hahn, K. I., Kavanagh, R. W., & Wrean, P. R. 1999, PhRvC, 60, 015801
Casella, C., Costantini, H., Lemut, A., et al. 2002, NuPhA, 706, 203
Caughlan, G. R., & Fowler, W. A. 1988, ADNDT, 40, 283
Coc, A., Goriely, S., Xu, Y., Saimpert, M., & Vangioni, E. 2011, ApJ, 744, 158
Coon, J. H. 1950, PhRv, 80, 488
Costello, D. G., Friesenhahn, S. J., & Lopez, W. M. 1970, NSE, 39, 409
Cyburt, R. H., Fields, B. D., Olive, K. A., & Yeh, T.-H. 2016, RvMP, 88, 015004
D’Agata, G., Pizzone, R. G., Cognata, M. L., et al. 2018, ApJ, 860, 61
Drosg, M., & Otuka, N. 2015, in Evaluation of the Absolute Angle-Dependent Differential Neutron Production Cross Sections by the Reactions 3H(p,n)3He, 1H(t,n)3He, 2H(d,n)3He, 3H(d,n)4He, and 2H(t,n)4He and of the Cross Sections of Their Time-Reversed Counterparts up to 30 MeV and Beyond, INDC(AUS)-0019 (Vienna: IAEA)
Ezer, D., & Cameron, G. W. 1962, Icar, 1, 422
Fields, B., & Sarkar, S. 2006, JPhG, 777, 208
Gibbons, J. H., & Macklin, R. L. 1959, PhRv, 114, 571
Guardo, G. L., Spitaleri, C., Lamia, L., et al. 2017, PhRvC, 95, 025807
Guardo, G. L., Spitaleri, C., Lamia, L., et al. 2019, EPJA, 55, 211
Gulino, M., Spitaleri, C., Cherubini, S., et al. 2010, JPhG, 37, 125105
Gulino, M., Spitaleri, C., Tang, X. D., et al. 2013, PhRvC, 87, 012801
Hayakawa, S., Cognata, M. L., Lamia, L., et al. 2021, ApJL, 915, L13
Israelian, G. 2012, Natur, 489, 37
Kolb, E. 2019, The Early Universe (Boca Raton, FL: CRC Press)
Komatsu, E., Smith, K. M., Dunkley, J., et al. 2011, ApJS, 192, 18
Korn, A. J., Grundahl, F., Richard, O., et al. 2006, Natur, 442, 657
La Cognata, M., Pizzone, R. G., José, J., et al. 2017, ApJ, 846, 65
Lamia, L., La Cognata, M., Spitaleri, C., Irgaziev, B., & Pizzone, R. G. 2012, PhRvC, 85, 025805
Lamia, L., Mazzocco, M., Pizzone, R. G., et al. 2019, ApJ, 879, 23
Lamia, L., Spitaleri, C., Bertulani, C. A., et al. 2017, ApJ, 850, 175
Lamia, L., Spitaleri, C., Carlin, N., et al. 2009, NCim, 031, 423
Lamia, L., Spitaleri, C., Tognelli, E., et al. 2015, ApJ, 811, 99
LUNA Collaboration, Bonetti, R., Broggini, C., et al. 1999, PhRvL, 82, 5205
MacFarlane, R., & Moller, P. 1997, Qtool: Calculation of Reactionq-values and Thresholds, Los Alamos National Laboratories—T-2 Nuclear Information Service, https://t2.lanl.gov/nis/data/qtool.html
Mossa, V., Stöckel, K., Cavanna, F., et al. 2020, Natur, 587, 210
n_TOF Collaboration, Barbagallo, M., Musumarra, A., et al. 2016, PhRvL, 117, 152701
Pettini, M., Zych, B. J., Murphy, M. T., Lewis, A., & Steidel, C. C. 2008, MNRAS, 391, 1499
Pitrou, C., Coc, A., Uzan, J.-P., & Vangioni, E. 2018, PhR, 754, 1
Pizzone, R. G., Bertulani, C. A., Lamia, L., et al. 2020a, EPJA, 56, 283
Pizzone, R. G., D’Agata, G., Cognata, M. L., et al. 2017, ApJ, 836, 57
Pizzone, R. G., Roeder, B. T., McCleskey, M., et al. 2016, EPJA, 52, 24
Pizzone, R. G., Spampinato, C., Spartá, R., et al. 2020b, EPJA, 56, 199
Pizzone, R. G., Spartá, R., Bertulani, C. A., et al. 2014, ApJ, 786, 112
Pizzone, R. G., Spitaleri, C., Bertulani, C. A., et al. 2013, PhRvC, 87, 025805
Rolfs, C. 2001, PrPNP, 46, 23
Smith, M. S., Kawano, L. H., & Malaney, R. A. 1993, ApJS, 85, 219
Spitaleri, C. 1991, in Problems of Fundamental Modern Physics, II: Proc. (Proc. Folgaria Meeting) ed. R. Cherubini, II, P. Dalpiaz, & B. Minetti (Singapore: World Scientific), 21
Spitaleri, C., Cherubini, S., Del Zoppo, A., et al. 2003, NuPhA, 719, C99
Spitaleri, C., La Cognata, M., Lamia, L., Pizzone, R. G., & Tumino, A. 2019, EPJA, 55, 161
Steigman, G. 2007, ARNPS, 57, 463
Tribble, R. E., Bertulani, C. A., Cognata, M. L., Mukhamedzhanov, A. M., & Spitaleri, C. 2014, RPPh, 77, 106901
Tumino, A., Bertulani, C. A., La Cognata, M., et al. 2021, ARNPS, 71, 345
Typel, S., & Baur, G. 2003, AnPhy, 305, 228
Typel, S., & Wolter, H. H. 2000, FBS, 29, 75
Weymann, R., & Moore, E. 1963, ApJ, 137, 552